Otolaryngology online journal

ISSN: 2250-0359 Volume 5 Issue 2 2015

Cochlear length determination in temporal bone specimens using histological serial Micro grinding imaging, micro computed tomography and flat-panel volumetric computed tomography

Waldemar Würfel[1], William F Burke[1], Thomas Lenarz[1] and Robert Kraemer[2]

[1]Department of Otolaryngology, Hannover Medical School, Carl-Neuberg-Str. 1, 30625 Hannover, Germany

Abstract

The cochlear length virtually describes the length of the cochlea in a straight line. Several theoretical options for measuring the length of the cochlea are conceivable. In choosing the type of cochlear implant electrode, this can play a crucial role. A wide range of electrodes is available, especially among the models designed to preserve residual hearing and structural integrity. It is believed that the depth of cochlear implant electrode insertion has an influence on the functional hearing based on the area of the cochlea that is electrically stimulated.

Method:

Imaging of nine human temporal bone specimens was performed using histological serial micro grinding imaging, micro computed tomography (microCT) and experimental flat-panel volumetric computed tomography (fpVCT). Measurements were then performed by outlining the cochlea in OsiriX (Pixmeo, Los Angeles USA). Results: The cochlear length of 9 human temporal bones was determined in each histological serial microgrinding imaging, fpVCT and microCT. Cochlear length ranges in histological serial grinding imaging from 45.3 mm to 38.7 mm, in microCT from 46.1 mm to 39.3 mm and in fpVCT from 45.8 mm to 39.8 mm. Significant inter- and intraindividual differences in the cochlear length were observed.

The presented methodology is capable of determining the cochlear length in each imaging modality.

Discussion:

A methodology to experimentally determine the cochlear length is interesting from both clinical and preclinical perspectives. Insertion studies are highly relevant to the development and evaluation of new electrode arrays. This study presents a measurement methodology that allows for individualized cochlear length measurement based on three established imaging modalities. The data presented here confirm differences in cochlear length. The method described here can be used to evaluate a cochlea in an experimental setting. This allows an individualized, pre-interventional evaluation of the specimen's specific cochlear anatomy and subsequently a personalized evaluation in cochlear implant insertion studies.

Introduction

A Cochlear Implant (CI) is an electronic device for the treatment of profound hearing loss or deafness. The CI replaces the damaged inner hair cells of the organ of Corti and electrically stimulates the spiral ganglion cells directly via an intra-cochlear electrode, ideally located in the scala tympani.

CIs are also indicated for the treatment of patients who are severely hearing impaired, but still have some useful residual hearing. In such patients a minimally traumatic implantation -both with regard to surgical technique as well as implant design- is recommended. In minimally traumatic CI surgery, preserving the integrity of the cochlear microstructure is essential.

The choice of the electrode plays a crucial role here [1]–[7] . The electrodes that are designed to preserve residual hearing are typically straight electrodes, which are positioned along the outer contour of the cochlea. They are available in different lengths, bending stiffnesses and number of contacts [8], [9]. With the ever-expanding indication range for treatment of patients with residual hearing with CI's the manufacturers have responded (as can be expected) by offering a portfolio of electrodes with different array lengths and diameters: personalized treatment is a central point of interest.

The length of the human cochlea is a poorly defined entity. Several methods have been introduced to measure the cochlear length (CL). Likewise the generally accepted landmarks used to define CL are numerous: the basilar membrane, spiral lamina or inner and outer bony rim of the cochlea, the choice of which often depends upon the imaging modality used in the study [10]–[20]. It has been chosen in this study to measure the length of the cochlea along the outer contour, as measured beginning from the round window membrane (anterior – superior) up to the helicotrema, as has been similarly described in previous histological studies[12], [16], [19], [21], [22]. As there is no formally accepted definition of CL, it seems prudent to establish a reliable, and easily performed method for doing just that. The goal of the current paper is to demonstrate that a consistent cochlear length can be measured using multiple high-resolution imaging modalities if a standardized procedure is employed. The study is designed as methodological translational research.

Methods

Imaging data was obtained from nine fresh human temporal bones embedded in epoxy resin. A total of 27 data stacks was acquired, made up of nine each from an experimental flat-panel volumetric computed tomograph (fpVCT – GE Corporate R&D), microCT and histological microgrinding imaging [23], [24]. The specimens were first scanned in an fpVCT at the Department of Diagnostic Radiology at Göttingen University Hospital. The scanning parameters corresponded to the values used throughout our former studies using fpVCT [25]–[29]. fpVCT consists of a modified circular CT gantry and two amorphous silicon flat-panel X-ray detectors, each measuring 20.5 x 20.5 cm with a 1024 x 1024 matrix of 200 mm detector elements [16]. The specimens were labelled utilizing sequential numeration together with the explanted side. As such, an identical specimen number indicates the same individual.

For micro CT imaging, the commercial desktop cone beam scanner µCT 80 (Scanco Medical AG, Brüttisellen, Switzerland) was used. The scanner consists of a micro focus X-ray source with 5 µm spot size and a detector providing 2048 x 128 elements (48 µm pitch), resulting in a resolution of 36 µm x 36 µm x 36 µm after reconstruction for specimens over 20 mm in diameter.

Histological serial microgrinding imaging is a highly accurate serial cross-sectional abrasive preparation technique, which is an adequate modality for imaging both soft and bony tissue structures with high contrast and spatial resolution. The imaging method is based on a custom-made device, in which the specimen surface can be abraded and sliced with micron precision.

The abrasion is documented using a tactile measuring device (Heidenhain Specto ST 3048, Heidenhain GmbH, Traunreut, Germany) with 2 µm resolution.

The acquired image sets were converted to the DICOM standard with full compatibility to conventional clinical DICOM viewers. The resulting voxel size corresponds to approximately 16 µm x 60 µm x 100 µm. This procedure has been previously published by our workgroup [23], [24].

The study was conducted in concordance with the principles of the Declaration of Helsinki and Good Clinical Practice. The use of the explanted human temporal bones was also approved by the local medical ethics committees of the Hannover Medical School (Hannover, Germany).

The imported DICOM data were then transferred to OsiriX MD and measured using 3D curved multiplanar reconstruction. The software's MPR interface provides 4 windows – one for each of 3 two-dimensional sections (each of which are oriented perpendicular to one another) and 1 additional window for the curved MPR, which is assembled based on the 3 two-dimensional views. The defined two-dimensional views are configured manually as follows: One is parallel to and passes through the basal turn of the cochlea, viewing it from the side; the second is placed at 90° to the first and passes through round window, viewing the cochlea from the other side; the third is centred on the modiolus and views the cochlea from above (fig. 1). This view of the cochlea has been published by Aschendorff et al. [21].

Figure 1: Starting point of the measurement (red dot): distal bony of the round window.

The curved MPR window uses the points defined manually along the outer wall of the cochlea to virtually unroll it and display the cochlea as a longitudinal tube in 2 dimensions as follows. The data points used to construct the curved MPR are defined by manually specifying locations along the outer edge of the bony cochlea in the 3 two-dimensional views along the projection of the osseous spiral lamina - or along the basilar membrane, in the case of histological samples (fig. 3 to 6, 8 and 9).

In all cases, the points of the measurement run from the outside edge of the bony rim of the round window (fig. 2) up to most apical and lateral point at the helicotrema (fig 6). The OsiriX software utilizes an algorithm to create a best-fit curve through the points defined in the previous step and establishes a curved MPR section which can be seen in the bottom right window in figures 4 through 6, 9 and 10. Figure 7a is 3D rendering of the cochlea in fpVCT and the manually set points along the lateral wall. Figure 7b illustrates the best fit curve through the set points and figure 7c the unrolled curve which is per definition the CL.

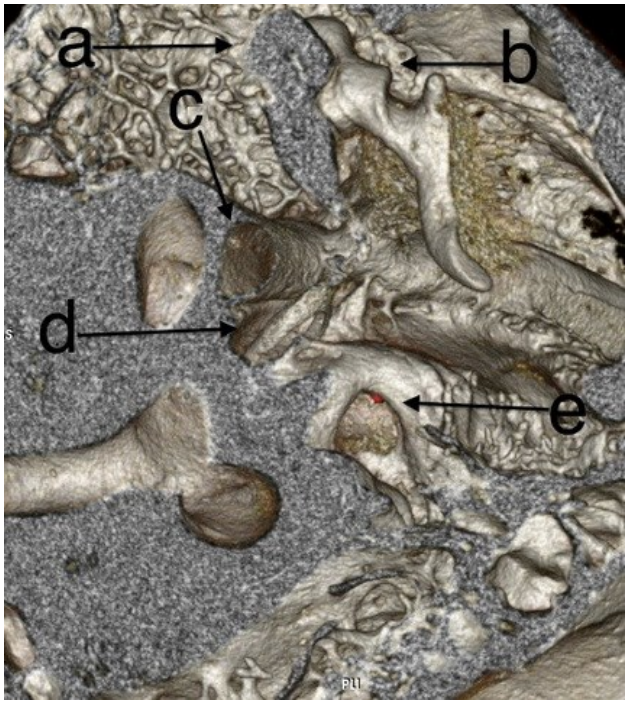

Figure 2: Starting point of the measurement (red dot): distal bony of the round window in 3D reconstruction of microCT data stack; a: medially dissected incus, b: malleus, c: facial nerve canal, d: stapes, e: round window.

The greater the number of points defined between the round window and the helicotrema, the smoother and more accurately shaped the curve along the lateral wall will be. Increasing the number of points reaches a threshold of diminishing returns: beyond a certain number of points no further change in the measured cochlear length is observed. This is used as the cut off for choosing the number of defined points necessary.

Statistical data were analysed by using paired and unpaired t-test.

Results

Table 1 shows the statistical data for each specimen and for each of the imaging modalities (histological serial microgrinding, microCT and fpVCT, respectively). In the histological serial microgrinding imaging the minimum mean length was measured at 38.7 mm in TB3R compared to a maximum length of 45.31 mm in TB4L, which results in a span length of 6.61 mm. For the microCT modality, the minimum mean length measured was 39.32 mm in TB3L with a maximum of 46.14 mm in TB5R, resulting in a span of 6.82 mm. The minimum length as measured in fpVCT was 39.84 mm in TB3L with a maximum of 45.83 mm in TB5R, yielding a span length of 5.99 mm.

Table 2 shows a comparison of means using an unpaired and paired t-test to determine whether a statistical significance in the measured lengths of the individual temporal bones is present in the three modalities. A paired t-test was used when comparing left and right side in the same specimen. Based on table 1 and 2, it can be seen that there are no statistically significant differences regarding histological serial microgrinding imaging in the lengths of TB4L and TB5R. In histological imaging samples can be arranged in the following order starting with the longest cochlea: TB5R (45.25 mm) and TB4L (45.31 mm) with no significant difference, TB2R (43.84 mm), TB4R (42.49 mm), TB5L (41.86 mm), TB1R (39.97 mm), TB3L (39.09 mm), TB1L (38.89 mm) and TB3R (38.7 mm).

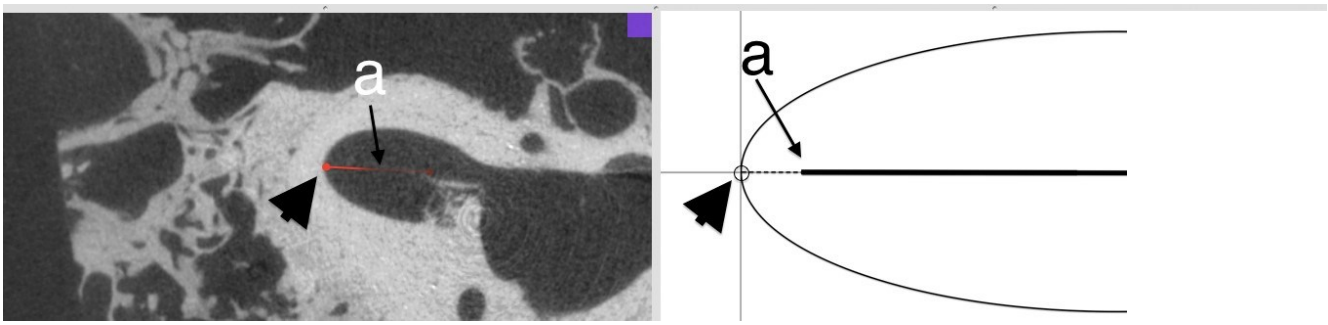

Figure 3: Curved measurement along the lateral wall of the cochlea in projection of the basilar

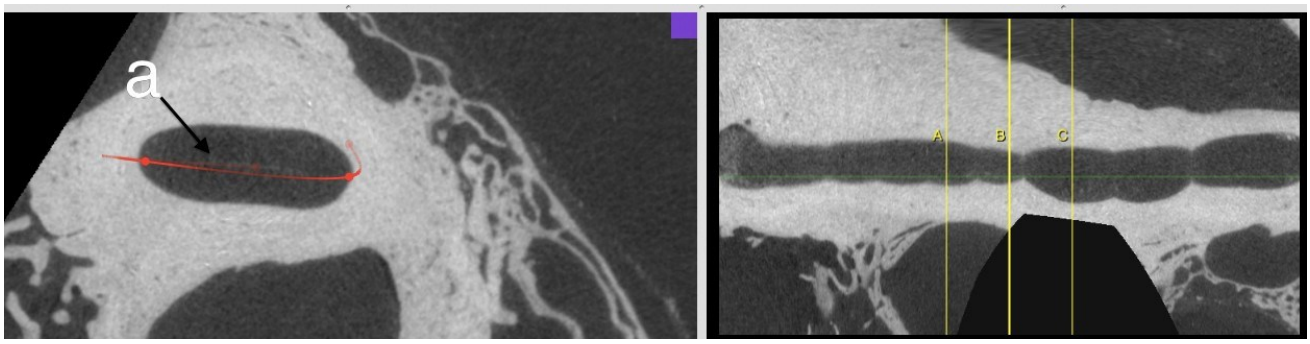

Figure 4: Curved measurement along the lateral wall of the cochlea in projection of the basilar

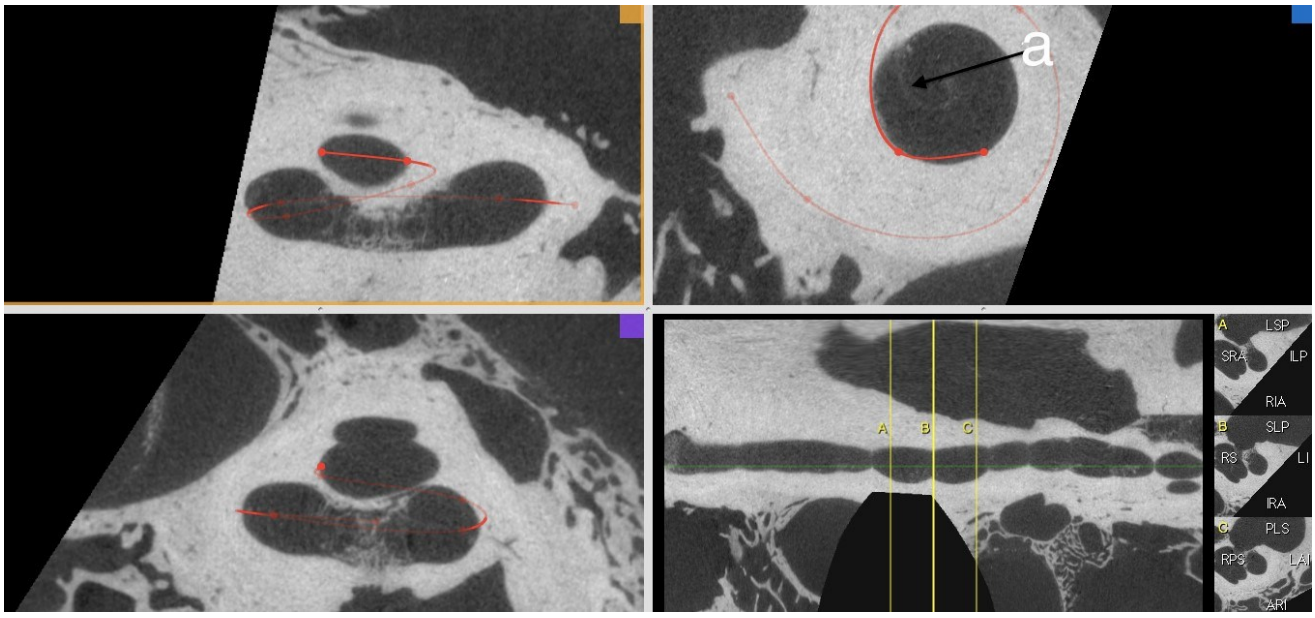

Figure 5: Curved measurement along the lateral wall of the cochlea in projection of the basilar

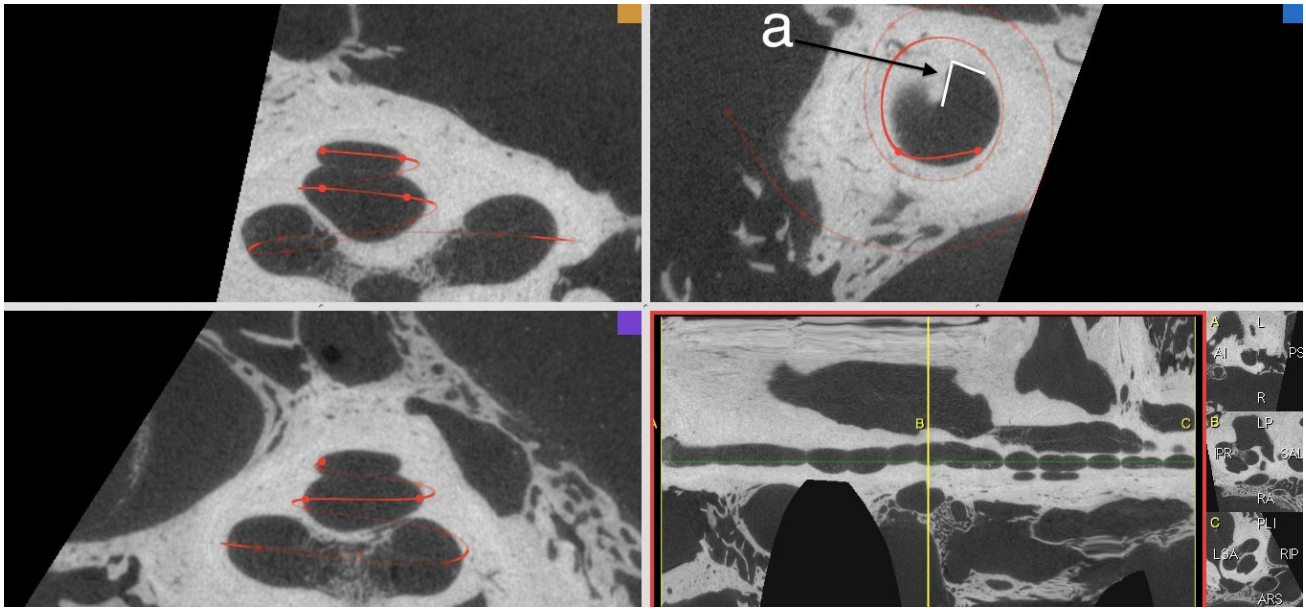

Figure 6: End point of the measurement (black arrow): helicotrema.

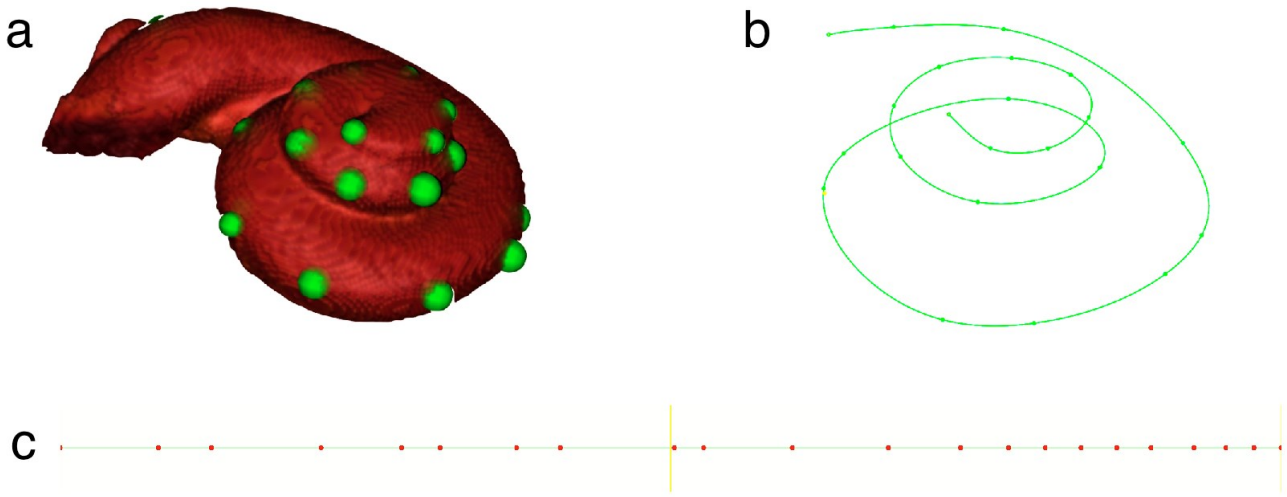

Figure 7: Illustration of three dimensional curve setting. a: 3D rendering oft the cochlea based on fpVCT data stack of TB4R. Green points in a are manually set along the outer wall. b: three dimensional best fitting curve through the

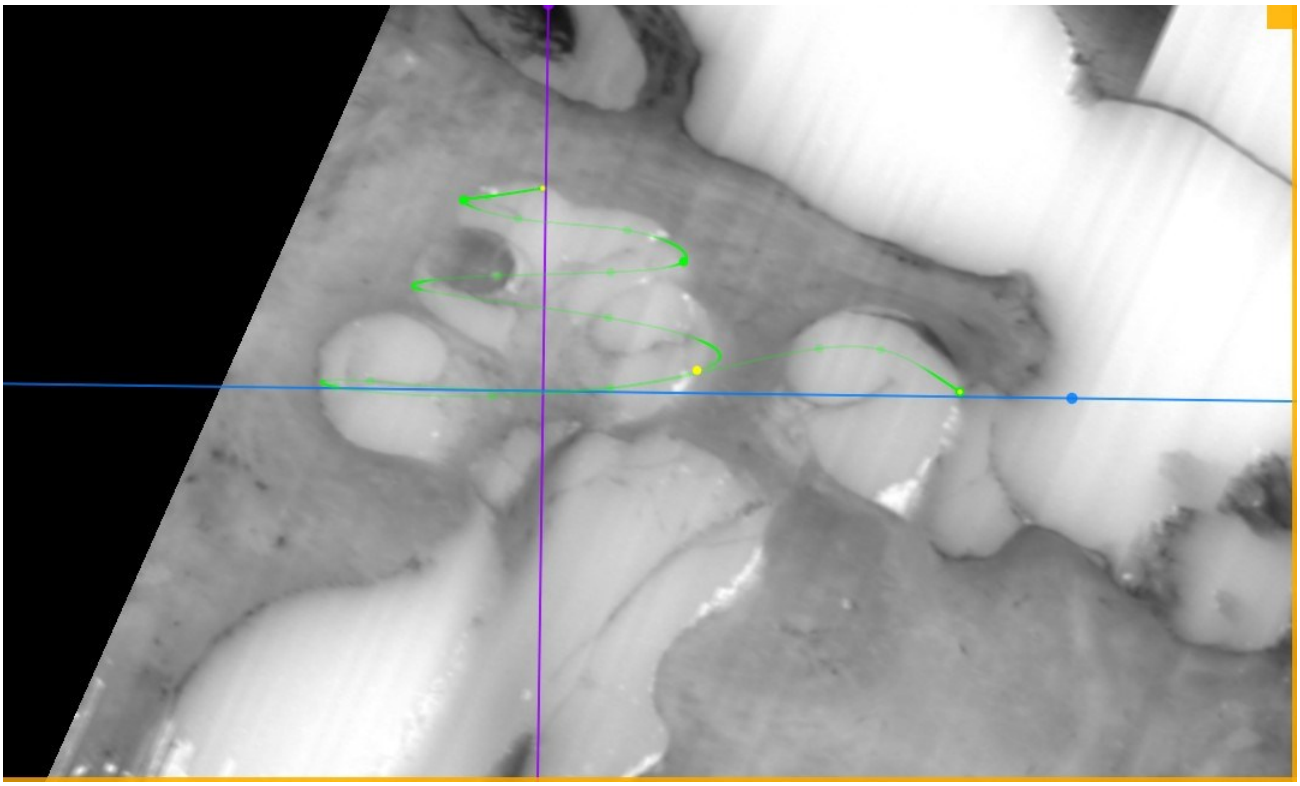

Figure 8: CL determination in histological serial microgrinding imaging.

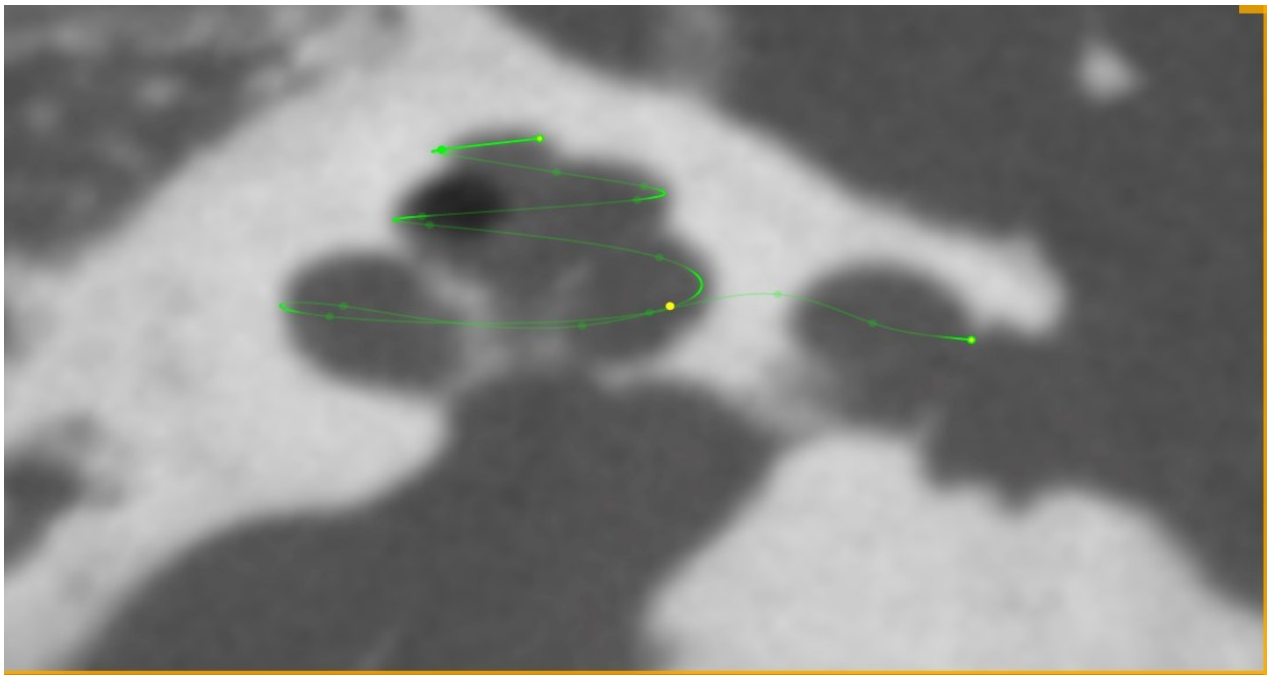

Figure 9: CL determination in fpVCT modality.

Table 1: Statistical data of 10 length measurements of each data stack

[mm]	Mean	Median	Std. Deviation	Variance	Maximum	Minimum	Range
Histology							
TB1L	38.89	38.85	.20	.039	39.2	38.7	.5
TB1R	39.97	40.05	.40	.160	40.3	38.9	1 4
TB2R	43.84	43.8	.14	.018	44,0	43.6	.4
TB3L	39.09	39.1	.14	.019	39.3	38.9	.4
TB3R	38.7	38.65	.17	.027	38.9	38.5	.4
TB4L	45.31	45.2	.16	.025	45.6	45.2	.4
TB4R	42.49	42.5	.23	.052	42.9	42.2	.7
TB5L	41.86	41.85	.15	.023	42.1	41.6	.7
TB5R	45.25	45.25	.16	.025	45.5	45,0	.7
microCT							
TB1L	40.25	40.25	.19	.036	40.6	40,0	0.6
TB1R	40.35	40.3	.25	.061	40.8	40,0	0.8
TB2R	44.41	44.3	.33	.110	45.3	44.1	1 2
TB3L	39.32	39.3	.41	.166	40.1	38.6	1 5
TB3R	40.47	40.45	.16	.025	40.7	40.3	.4
TB4L	44.59	44.5	.29	.081	45,0	44.2	.8
TB4R	42.97	43.05	.24	.058	43.2	42.5	.7
TB5L	42.0	42.2	.80	.633	42.5	39.8	2 7
TB5R	46.14	46.1	.16	.025	46.4	45.9	.5
fpVCT							
TB1L	40.9	40.95	.30	.091	41.3	40.4	.9
TB1R	40.45	40.5	.15	.023	40.7	40.2	.5
TB2R	43.44	43.45	.20	.038	43.7	43,0	.7
TB3L	39.84	39.85	.17	.027	40.1	39.6	.5
TB3R	40.48	40.5	.13	.017	40.7	40.3	.4
TB4L	45.5	45.55	.21	.042	45.7	45,0	.7
TB4R	43.0	43.1	.18	.033	43.2	42.6	.6
TB5L	42.55	42.6	.15	.023	42.7	42.2	.5
TB5R	45.83	45.85	.16	.025	46.1	45.6	.5

		Histo	mCT	fpVCT
		p-value		
TB1L	TB1R	.000*	.588*	.003*
	TB2R	.000	.000	.000
	TB3L	.017	.001	.000
	TB3R	.03	.863	.002
	TB4L	.000	.000	.000
	TB4R	.000	.000	.000
	TB5L	.000	.001	.000
	TB5R	.000	.000	.000
TB1R	TB2R	.000	.000	.000
	TB3L	.000	.000	.000
	TB3R	.000	.21	.641
	TB4L	.000	.000	.000
	TB4R	.000	.000	.000
	TB5L	.000	.000	.000
	TB5R	.000	.000	.000
TB2R	TB3L	.000	.000	.000
	TB3R	.000	.000	.000
	TB4L	.000	.209	.000
	TB4R	.000	.000	.000
	TB5L	.000	.000	.000
	TB5R	.000	.000	.000
TB3L	TB3R	.000*	.000*	.000*
	TB4L	.000	.000	.000
	TB4R	.000	.000	.000
	TB5L	.000	.000	.000
	TB5R	.000	.000	.000
TB3R	TB4L	.000	.000	.000
	TB4R	.000	.000	.000
	TB5L	.000	.000	.000
	TB5R	.000	.000	.000
TB4L	TB4R	.000*	.000*	.000*
	TB5L	.000	.000	.000
	TB5R	.409	.000	.001
TB5L	TB5R	.000*	.000	.000*

Table 2: Comparison of means using paired (*) and unpaired t-test from one specimen to another in histological serial microgrinding imaging, mCT and fpVCT.

One can similarly use tables 1 and 2 to examine the CL using the microCT imaging modality. This leads to following order starting with longest cochlea: TB5R (46.14 mm), TB4L (44.59 mm) and TB2R (44.41 mm) with no significant difference, TB4R (42.97 mm), TB5L (42.0 mm), TB3R (40.47 mm) as well as TB1R (40.35 mm) and TB1L (40.25 mm) with no significant difference and shortest CL in TB3L (39.32 mm).

The same principle can be applied to the fpVCT modality using tables 1 and 2 leading to following order of CL starting with the longest: TB5R (45.83 mm), TB4L (45.5 mm), TB2R (43.44 mm), TB4R (43.0 mm), TB5L (42.55 mm), TB1L (40.9 mm), TB3R (40.48mm) and TB1R (40.45mm) with no significant difference and as shortest CL TB3L (39.84 mm).

Table 3 utilizes a paired t-test ($p = .05$) to compare the means obtained for the individual samples between the different imaging modalities. 10 measurements of one specimen are compared from one modality to the same specimen to the other modalities. No significant differences were observed between the measurements obtained between microCT and histological imaging in TB1R, TB3L and TB5L. Similarly, no differences were seen using microCT and fpVCT in TB1R, TB3R and TB4R. As well there were no significant differences between fpVCT and histological imaging in TB4L ($p = .076$).

Discussion

Cochlear length is an often used but seldom clearly defined entity. Its importance has been mentioned – among other places – in clinical and preclinical settings of CI insertion studies [1]–[3], [5], [6], [20]. Evidence has shown a relationship between decreased speech perception and short insertion depth on the one hand [30], while on the other hand, deeper insertion has been associated with a significant reduction in the ability to preserve residual hearing [31]–[37].

Adunka et al. [38] observed indirect indications of interindivdual differences in the length of the scala tympani by comparing electrode placement in specimens after CI-insertion in experimental setting. They determined that using the manufacturer's data for insertion depth did not lead to comparable intracochlear placement. On the contrary, they observed significantly different insertion angles.

Literature research shows founded evidence for individual CL differences [10]–[20]. Despite this, there is as yet no standardized method for determining the desired insertion depth of CI electrodes preoperatively. It is therefore critical to establish a methodology for determining CL preinterventionally to enable prudent decisions with regard to electrode choice, allowing the patient's anatomy to complement the audiological data in this endeavour.

Table 3: Comparison of means of one imaging modality to each other by using paired t-test.

	Histology [mm]	microCT [mm]	p-value	microCT [mm]	fpVCT [mm]	p-value	fpVCT [mm]	Histology [mm]	p-value
TB1L	38.89	40.25	.000	40.25	40.9	.000	40.9	38.89	.000
TB1R	39.97	40.35	.057	40.35	40.45	.195	40.45	39.97	.008
TB2R	43.84	44.41	.001	44.41	43.44	.000	43.44	43.84	.001
TB3L	39.09	39.32	.174	39.32	39.84	.007	39.84	39.09	.000
TB3R	38.7	40.47	.000	40.47	40.48	.899	40.48	38.7	.000
TB4L	45.31	44.59	.000	44.59	45.5	.000	45.5	45.31	.076
TB4R	42.49	42.97	.002	42.97	43.0	.776	43.0	42.49	.000
TB5L	41.86	42.0	.619	42.0	42.55	.047	42.55	41.86	.000
TB5R	45.25	46.14	.000	46.14	45.83	.000	45.83	45.25	.000

Several methods for determining CL are in common practice in an experimental setting. Miller et al [10]mention four methods for determining CL and length of the organ of Corti (COL) and are summarized below.

The surface preparation method described by Bredberg et al [39] ,Ulehlova et al [13] and Wright et al [40] is a dissection-based microscopic approach in which inner and outer hair cells are stained, counted and measured in their extent.

The Guild method [14] was introduced in 1921 and later modified by Schuknecht in 1953 [15] and involves a serial histological dissection method that considers the COL in each individual dissected section and reassembles it into a complete organ.

Sato et al measured the COL in 1991 using individual histological celloidin slides and then virtually reconstructing them using a software-based approach [11] (histological 3D reconstruction method). They observed significant sexual dimorphism with a COL of 37.1 mm in males and 32.3 mm in females.

There are computed tomography (CT) and magnetic resonance imaging (MRI)-based methodologies that have evolved due to the progress of technology. They are generally based on a volume generated using one or both of these modalities. Using landmarks within the volume, distance measurements can be performed [12], [20], [22], [41]–[44].

Miller et al found no significant differences in the average COL between males and females by reviewing three histological and one CT-based method. He found an average COL of 34 mm and 33 mm in males and females, respectively. The discrepancy between Miller's and Sato's findings may lie in the different modalities used in their studies. Conventional histological sections are subject to process-dependent distortion in images, which has to be taken into account.

Histological serial microgrinding imaging does not, in principle, fall into one of the above-listed categories. It is a highly accurate serial cross-sectional abrasive preparation technique, which is an adequate modality for imaging both soft and bony tissue structures with high contrast and spatial resolution [Ref Rau]. The process is based on taking serial images of a temporal bone sample that has been previously fixed in an epoxy resin. It is then sequentially and precisely abraded and the sequential images taken. The distance and orthogonality of the image layer are controlled by high-precision measurement techniques. This results in the generation of a defined image stack of known, verifiable metric dimensions [23], [24]

A high precision 3D curved MPR measurement tool with proven, reproducible results is integrated in the OsiriX software suite OsiriX is an open-source software package for Mac OS X [45], [46], which is increasingly used in medical imaging evaluation [47]–[49].

It is an intensively functional program for 3D reconstruction and measurements using DICOM data. The imaging modalities described in this paper are state of the art experimental methods with unmatched imaging quality of the bony inner ear architecture.

Experimental fpVCT represents a methodological bridge to the clinically established and approved cone beam CT (CBCT). However, microCT and histological serial microgrinding imaging are essentially experimental techniques. MicroCT is widely used in experimental high-resolution imaging of the temporal bone [41], [44], [50]–[54]. Histological serial microgrinding imaging allowed the CL measurements to be performed in a high-precision 3D data stack with approved, unique and unmatched quality [23], [24].

Our research here involved a systematic approach beginning with high-precision histology, moving on to high-resolution x-ray CT (microCT) and then on to volume tomography (fpVCT), the latter method being directly adjacent to the clinically established CBCT modality. As such the perspective of applying this technique to the clinically available CBCT appears promising. Nevertheless, the clinical application has not been adequately evaluated yet.

In this study, each cochlea in the 27 data stacks was measured ten times to ensure a valid mean value (see table 1). This was performed using the 3D curved MPR measurement tool.

The technique presented here is not only an estimation, but rather a specific individual determination (see figures 1 and 3 to 9).

The paired comparison of two imaging modalities measuring the same sample (see table 3) detected significant differences and analogies in the three modalities in between the same specimen. The main reasons for the differences may be partial volume effects in MPR. Voxels in microCT and fpVCT are isotropic, in comparison to the anisotropic voxels in the microgrinding imaging (16 µm x 16 µm x 100 µm). This may have led to different absolute lengths in the MPR measurement. Each imaging modality has its specific charecteristic in resolution and depiction. That is why the standard deviation in measurements is relevant. The standard deviation in histological imaging ranges from .15 mm to .23 mm and in fpVCT imaging from .13 mm to .3 mm. In microCT is a standard deviation from .16 mm to .8 mm which seems to be a wide variation in measurement for TB5L (tab. 1). Inbetween the 10 measurements for TB5L is one value of 39.8 mm that is far off the mean value. Regarding this as outlier the standard deviation for TB5L in microCT would be .2 mm and the maximum standard deviation in microCT in total .41 mm.

Therefore, the presented method is capable of reproducibly determining the CL in between the used imaging modalities for human temporal bones in an experimental setting. This could be shown in the small standard deviation for the CL (tab. 1) and the significant differences in t-test for the means in between the three modalities for the same specimen (tab. 2).

Results show that TB5R and TB4L are significantly considered as longest cochleae in all imaging modalities and that there is an increment in CL from TB5R to TB4L, TB2R, TB4R and TB5L. TB1R, TB1L, TB3R and TB4L can be considered as shortest cochleae with a clear ranking at least in between modalities.

Mean distances between the CL for each modality and specimen differ in a maximum of 2.01 mm (TB1L) and a minimum of .19 mm (TB4L) between fpVCT and histological imaging. Comparing CL of histological imaging to microCT there is a maximum difference of 1.36 mm (TB1L) and a minimum of .14 mm (TB5L). Similarly between microCT and fpVCT there is a maximum difference of .91 mm and am minimum of .03 mm.

In summary it can be deducted from these data that there is a non negligible variation in between the modalities but also a high correlation and small standard deviation within the modalities. This means that the single imaging modalities lead to a reproducible result in CL determination and will give a significant CL in a temporal bone specimen.

Knowledge about the CL is crucial in CI research and is therefore a topic of intense research. The recognized tonotopy along the basilar membrane and spiral ganglion cells has led to the utilization of the pure tone audiogram as a tool for choosing the type of CI array. But further considerations must be taken into account when preserving the structural integrity of the cochlear anatomy is an issue [7,8].

These concerns are based on the understanding that a deeper insertion may lead to trauma to the basilar membrane, as the scala tympani narrows apically.

There are only few methods to determine the CL preinterventionally in an experimental setting [22], [44], [55]. Especially Erixon et al reported in 2013 on their previous corrosion cast studies in wich they estimated the CL that an Archimedean curve as used by them will lead to wrong estimations in cochleae which are not within in the standard deviation of a normally distributed CL [55]. Their method is suited to estimate the basal turn length but is indeed no measurement method itself.

Metric analysis of the cochlear anatomy without changing the anatomy itself through preparation techniques is of central preclinical clinical importance. On the one hand up to now preclinical CI insertion studies are rarely performed with individualized determination of the CL. On the other hand different individual CL and anatomy is a known topic as listed in previous paragraphs.

There is no evidence that identical implantation in two different human cochleae with the same CI array length will result in identical positioning in terms of insertion depth or angle. Indeed, there are contrariwise indirect signs for interindividual differences in CL when the insertion depths are measured as shown by Adunka et al [38].

The significance of tailoring the array to the patient can be observed in the reaction of manufacturers. New arrays do have various lengths such as the Nucleus Cochlear Hybrid L (16 mm), the Nucleus Cochlear CI422 (20 mm) and the Med-El Flex (20 mm, 24 mm and 28 mm and 31,5 mm) series are manufacturer's answer to the problem of tailoring the arrays to new audiological indications [8], [9].

These electrodes regard indirectly to the CL without a reliable methodology to measure the CL whether in preclinical nor in clinical setting.

Harming the basilar membrane by CI operation leads to a loss of residual hearing that is beneficial to CI patients [56]–[60]. Therefore, special electrodes were designed to preserve residual hearing. These are typically thin straight electrodes without a stylet, which are positioned through the round window along the outer wall of the cochlea within the scala tympani.

The presented method considers this characteristic of electrode placement. Starting point of the measurement is the round window as well the fitting of the curve for CL determination is along the outer cochlear wall up to the helicotrema. This measurement is therefore especially suited for evaluation in insertion studies for lateral wall arrays. The presented data support evidence for different CL in human cochleae which should be enforced to adapt in CI research wherever possible. Consequent consideration of the CL in CI array development may have presumably an impact on electrode design in general.

[1] R. K. Shepherd, G. M. Clark, B. C. Pyman, and R. L. Webb, “Banded intracochlear electrode array: evaluation of insertion trauma in human temporal bones,” Ann. Otol. Rhinol. Laryngol., vol. 94, no. 1 Pt 1, pp. 55–59, Feb. 1985.

[2] D. B. Welling, R. Hinojosa, B. J. Gantz, and J. T. Lee, “Insertional trauma of multichannel cochlear implants,” Laryngoscope, vol. 103, no. 9, pp. 995–1001, Sep. 1993.

[3] D. W. Kennedy, “Multichannel intracochlear electrodes: mechanism of insertion trauma,” Laryngoscope, vol. 97, no. 1, pp. 42–49, Jan. 1987.

[4] O. Adunka, W. Gstoettner, M. Hambek, M. H. Unkelbach, A. Radeloff, and J. Kiefer, “Preservation of basal inner ear structures in cochlear implantation,” ORL J. Oto-Rhino-Laryngol. Its Relat. Spec., vol. 66, no. 6, pp. 306–312, 2004.

[5] O. Adunka, J. Kiefer, M. H. Unkelbach, A. Radeloff, and W. Gstoettner, “Evaluating cochlear implant trauma to the scala vestibuli,” Clin. Otolaryngol. Off. J. ENT-UK Off. J. Neth. Soc. Oto-Rhino-Laryngol. Cervico-Facial Surg., vol. 30, no. 2, pp. 121–127, Apr. 2005.

[6] [6] P. Wardrop, D. Whinney, S. J. Rebscher, W. Luxford, and P. Leake, “A temporal bone study of insertion trauma and intracochlear position of cochlear implant electrodes. II: Comparison of Spiral Clarion and HiFocus II electrodes.,” Hear Res, vol. 203, no. 1–2, pp. 68–79, May 2005.

[7] W. Gstöttner, S.-M. Pok, S. Peters, J. Kiefer, and O. Adunka, “[Cochlear implantation with preservation of residual deep frequency hearing],” HNO, vol. 53, no. 9, pp. 784–790, Sep. 2005.

[8] The New FLEX Portfolio. 2012.

[9] CochlearTM, “Cochlear Nucleus Electrode Portfolio.” .

[10] J. D. Miller, “Sex differences in the length of the organ of Corti in humans,” J. Acoust. Soc. Am., vol. 121, no. 4, pp. EL151–155, Apr. 2007.

[11] H. Sato, I. Sando, and H. Takahashi, “Sexual dimorphism and development of the human cochlea. Computer 3-D measurement,” Acta Otolaryngol. (Stockh.), vol. 111, no. 6, pp. 1037–1040, 1991.

[12] E. Erixon, H. Hogstorp, K. Wadin, and H. Rask-Andersen, “Variational Anatomy of the Human Cochlea: Implications for Cochlear Implantation. [Miscellaneous Article],” Otol. Neurotol. January 2009, vol. 30, no. 1, pp. 14–22, 2009.

[13] L. Ulehlová, L. Voldrich, and R. Janisch, “Correlative study of sensory cell density and cochlear length in humans,” Hear. Res., vol. 28, no. 2–3, pp. 149–151, 1987.

[14] S. R. Guild, “A graphic reconstruction method for the study of the organ of Corti,” Anat Rec, vol. 22, p. 141â€“157, 1921.

[15] H. F. SCHUKNECHT, “Techniques for study of cochlear function and pathology in experimental animals; development of the anatomical frequency scale for the cat.,” AMA Arch Otolaryngol, vol. 58, no. 4, pp. 377–397, Oct. 1953.

[16] A. Kawano, H. L. Seldon, and G. M. Clark, “Computer-aided three-dimensional reconstruction in human cochlear maps: measurement of the lengths of organ of Corti, outer wall, inner wall, and Rosenthal’s canal,” Ann. Otol. Rhinol. Laryngol., vol. 105, no. 9, pp. 701–709, Sep. 1996.

[17] M. Hardy, “The length of the organ of Corti in man,” Am. J. Anat., vol. 62, no. 2, pp. 291–311, 1938.

[18] A. Takagi and I. Sando, “Computer-aided three-dimensional reconstruction: a method of measuring temporal bone structures including the length of the cochlea,” Ann. Otol. Rhinol. Laryngol., vol. 98, no. 7 Pt 1, pp. 515–522, Jul. 1989.

[19] B. Escudé, C. James, O. Deguine, N. Cochard, E. Eter, and B. Fraysse, “The size of the cochlea and predictions of insertion depth angles for cochlear implant electrodes,” Audiol. Neurootol., vol. 11 Suppl 1, pp. 27–33, 2006.

[20] B. M. Verbist, L. Ferrarini, J. J. Briaire, A. Zarowski, F. Admiraal-Behloul, H. Olofsen, J. H. C. Reiber, and J. H. M. Frijns, “Anatomic Considerations of Cochlear Morphology and Its Implications for Insertion Trauma in Cochlear Implant Surgery. [Miscellaneous Article],” Otol. Neurotol. June 2009, vol. 30, no. 4, pp. 471–477, 2009.

[21] A. Aschendorff, “Imaging in cochlear implant patients,” GMS Curr. Top. Otorhinolaryngol. Head Neck Surg., vol. 10, Apr. 2012.

[22] H. Rask-Andersen, W. Liu, E. Erixon, A. Kinnefors, K. Pfaller, A. Schrott-Fischer, and R. Glueckert, “Human cochlea: anatomical characteristics and their relevance for cochlear implantation,” Anat. Rec. Hoboken NJ 2007, vol. 295, no. 11, pp. 1791–1811, Nov. 2012.

[23] T. S. Rau, W. Würfel, T. Lenarz, and O. Majdani, “Three-dimensional histological specimen preparation for accurate imaging and spatial reconstruction of the middle and inner ear,” Int. J. Comput. Assist. Radiol. Surg., vol. 8, no. 4, pp. 481–509, Jul. 2013.

[24] T. S. Rau, A. Hussong, A. Herzog, O. Majdani, T. Lenarz, and M. Leinung, “Accuracy of computer-aided geometric 3D reconstruction based on histological serial microgrinding preparation.,” Comput Methods Biomech Biomed Engin, p. 1, Nov. 2010.

[25] J. Missbach-Guentner, C. Dullin, M. Zientkowska, M. Domeyer-Missbach, S. Kimmina, S. Obenauer, F. Kauer, W. Stühmer, E. Grabbe, W. F. Vogel, and F. Alves, “Flat-panel detector-based volume computed tomography: a novel 3D imaging technique to monitor osteolytic bone lesions in a mouse tumor metastasis model,” Neoplasia New York N, vol. 9, no. 9, pp. 755–765, Sep. 2007.

[26] S. H. Bartling, O. Majdani, R. Gupta, T. Rodt, C. Dullin, P. F. Fitzgerald, and H. Becker, “Large scan field, high spatial resolution flat-panel detector based volumetric CT of the whole human skull base and for maxillofacial imaging.,” Dentomaxillofac Radiol, vol. 36, no. 6, pp. 317–327, Sep. 2007.

[27] S. H. Bartling, R. Gupta, A. Torkos, C. Dullin, G. Eckhardt, T. Lenarz, H. Becker, and T. Stöver, “Flat-panel volume computed tomography for cochlear implant electrode array examination in isolated temporal bone specimens.,” Otol Neurotol, vol. 27, no. 4, pp. 491–498, Jun. 2006.

[28] O. Majdani, S. H. Bartling, M. Leinung, T. Stöver, M. Lenarz, C. Dullin, and T. Lenarz, “Image-guided minimal-invasive cochlear implantation–experiments on cadavers,” Laryngo-rhinootologie, vol. 87, no. 1, pp. 18–22, Jan. 2008.

[29] O. Majdani, S. H. Bartling, M. Leinung, T. Stöver, M. Lenarz, C. Dullin, and T. Lenarz, “A true minimally invasive approach for cochlear implantation: high accuracy in cranial base navigation through flat-panel-based volume computed tomography.,” Otol Neurotol, vol. 29, no. 2, pp. 120–123, Feb. 2008.

[30] I. Hochmair, W. Arnold, P. Nopp, C. Jolly, J. Müller, and P. Roland, “Deep electrode insertion in cochlear implants: apical morphology, electrodes and speech perception results,” Acta Otolaryngol. (Stockh.), vol. 123, no. 5, pp. 612–617, Jun. 2003.

[31] P. Boyd, “Potential Benefits From Deeply Inserted Cochlear Implant Electrodes,” Ear Hear. JulyAugust 2011, vol. 32, no. 4, pp. 411–427, 2011.

[32] W. Gstoettner, H. Plenk Jr, P. Franz, J. Hamzavi, W. Baumgartner, C. Czerny, and K. Ehrenberger, “Cochlear implant deep electrode insertion: extent of insertional trauma,” Acta Otolaryngol. (Stockh.), vol. 117, no. 2, pp. 274–277, Mar. 1997.

[33] W. Gstoettner, S.-M. Pok, S. Peters, J. Kiefer, and O. Adunka, “[Cochlear implantation with preservation of residual deep frequency hearing].,” HNO, vol. 53, no. 9, pp. 784–790, Sep. 2005.

[34] W. K. Gstoettner, W. D. Baumgartner, P. Franz, and J. Hamzavi, “Cochlear implant deep-insertion surgery.,” Laryngoscope, vol. 107, no. 4, pp. 544–546, Apr. 1997.

[35] A. V. Hodges, E. Villasuso, T. Balkany, P. A. Bird, S. Butts, D. Lee, and O. Gomez, “Hearing results with deep insertion of cochlear implant electrodes.,” Am J Otol, vol. 20, no. 1, pp. 53–55, Jan. 1999.

[36] H. Skarzynski, A. Lorens, M. Zgoda, A. Piotrowska, P. H. Skarzynski, and A. Szkielkowska, “Atraumatic round window deep insertion of cochlear electrodes.,” Acta Otolaryngol, vol. 131, no. 7, pp. 740–749, Jul. 2011.

[37] S. Tamir, E. Ferrary, S. Borel, O. Sterkers, and A. Bozorg Grayeli, “Hearing preservation after cochlear implantation using deeply inserted flex atraumatic electrode arrays.,” Audiol Neurootol, vol. 17, no. 5, pp. 331–337, 2012.

[38] O. Adunka, M. H. Unkelbach, M. G. Mack, A. Radeloff, and W. Gstoettner, “Predicting basal cochlear length for electric-acoustic stimulation.,” Arch Otolaryngol Head Neck Surg, vol. 131, no. 6, pp. 488–492, Jun. 2005.

[39] G. Bredberg, “Cellular pattern and nerve supply of the human organ of Corti.,” Acta Otolaryngol, p. Suppl 236:1+, 1968.

[40] A. Wright, A. Davis, G. Bredberg, L. Ulehlova, and H. Spencer, “Hair cell distributions in the normal human cochlea.,” Acta Otolaryngol Suppl, vol. 444, pp. 1–48, 1987.

[41] J. I. Lane, R. J. Witte, C. L. W. Driscoll, J. J. Camp, and R. A. Robb, “Imaging microscopy of the middle and inner ear: Part I: CT microscopy.,” Clin Anat, vol. 17, no. 8, pp. 607–612, Nov. 2004.

[42] J. I. Lane, R. J. Witte, O. W. Henson, C. L. W. Driscoll, J. Camp, and R. A. Robb, “Imaging microscopy of the middle and inner ear: Part II: MR microscopy.,” Clin Anat, vol. 18, no. 6, pp. 409–415, Sep. 2005.

[43] G. M. Fatterpekar, A. H. Doshi, M. Dugar, B. N. Delman, T. P. Naidich, and P. M. Som, “Role of 3D CT in the evaluation of the temporal bone.,” Radiographics, vol. 26 Suppl 1, pp. S117–S132, Oct. 2006.

[44] L. Ferrarini, B. M. Verbist, H. Olofsen, F. Vanpoucke, J. H. M. Frijns, J. H. C. Reiber, and F. Admiraal-Behloul, “Autonomous virtual mobile robot for three-dimensional medical image exploration: Application to micro-CT cochlear images,” Artif. Intell. Med., vol. 43, no. 1, pp. 1–15, May 2008.

[45] OsiriX DICOM-Viewer. 2010.

[46] A. Rosset, L. Spadola, and O. Ratib, “OsiriX: an open-source software for navigating in multidimensional DICOM images.,” J Digit Imaging, vol. 17, no. 3, pp. 205–216, Sep. 2004.

[47] G. Kim, H.-J. Jung, H.-J. Lee, J.-S. Lee, S. Koo, and S.-H. Chang, “Accuracy and Reliability of Length Measurements on Three-Dimensional Computed Tomography Using Open-Source OsiriX Software.,” J Digit Imaging, vol. 25, no. 4, pp. 486–491, Aug. 2012.

[48] G. Melissano, L. Bertoglio, V. Civelli, A. C. M. Amato, G. Coppi, E. Civilini, G. Calori, F. D. Cobelli, A. D. Maschio, and R. Chiesa, “Demonstration of the Adamkiewicz artery by multidetector computed tomography angiography analysed with the open-source software OsiriX.,” Eur J Vasc Endovasc Surg, vol. 37, no. 4, pp. 395–400, Apr. 2009.

[49] Y.-C. Wang, Y.-C. Liu, T.-C. Hsieh, S.-T. Lee, and M.-L. Li, “Aneurysmal subarachnoid hemorrhage diagnosis with computed tomographic angiography and OsiriX.,” Acta Neurochir Wien, vol. 152, no. 2, pp. 263–9; discussion 269, Feb. 2010.

[50] K. Engelke, M. Karolczak, A. Lutz, U. Seibert, S. Schaller, and W. Kalender, “Micro-CT. Technology and application for assessing bone structures,” Radiologe, vol. 39, no. 3, pp. 203–212, Mar. 1999.

[51] D. A. Gerneke, G. B. Sands, R. Ganesalingam, P. Joshi, B. J. Caldwell, B. H. Smaill, and I. J. Legrice, “Surface imaging microscopy using an ultramiller for large volume 3D reconstruction of wax- and resin-embedded tissues.,” Microsc Res Tech, vol. 70, no. 10, pp. 886–894, Oct. 2007.

[52] G. J. Wiet, P. Schmalbrock, K. Powell, and D. Stredney, “Use of ultra-high-resolution data for temporal bone dissection simulation.,” Otolaryngol Head Neck Surg, vol. 133, no. 6, pp. 911–915, Dec. 2005.

[53] H. Uzun, I. S. Curthoys, and A. S. Jones, “A new approach to visualizing the membranous structures of the inner ear - high resolution X-ray micro-tomography.,” Acta Otolaryngol, vol. 127, no. 6, pp. 568–573, Jun. 2007.

[54] A. Postnov, A. Zarowski, N. D. Clerck, F. Vanpoucke, F. E. Offeciers, D. V. Dyck, and S. Peeters, “High resolution micro-CT scanning as an innovative tool for evaluation of the surgical positioning of cochlear implant electrodes.,” Acta Otolaryngol, vol. 126, no. 5, pp. 467–474, May 2006.

[55] E. Erixon and H. Rask-Andersen, “How to predict cochlear length before cochlear implantation surgery,” Acta Otolaryngol. (Stockh.), pp. 1–8, Sep. 2013.

[56] T. Lenarz, C. James, D. Cuda, A. Fitzgerald O’Connor, B. Frachet, J. H. M. Frijns, T. Klenzner, R. Laszig, M. Manrique, M. Marx, P. Merkus, E. A. M. Mylanus, E. Offeciers, J. Pesch, A. Ramos-Macias, A. Robier, O. Sterkers, and A. Uziel, “European multi-centre study of the Nucleus Hybrid L24 cochlear implant,” Int. J. Audiol., pp. 1–11, Sep. 2013.

[57] A. Büchner, M. Schüssler, R. D. Battmer, T. Stöver, A. Lesinski-Schiedat, and T. Lenarz, “Impact of low-frequency hearing,” Audiol. Neurootol., vol. 14 Suppl 1, pp. 8–13, 2009.

[58] H. Skarzynski, A. Lorens, M. Matusiak, M. Porowski, P. H. Skarzynski, and C. J. James, “Cochlear Implantation With the Nucleus Slim Straight Electrode in Subjects With Residual Low-Frequency Hearing,” Ear Hear., Jan. 2014.

[59] M. K. Cosetti, D. R. Friedmann, B. Z. Zhu, S. E. Heman-Ackah, Y. Fang, R. G. Keller, W. H. Shapiro, J. T. Roland Jr, and S. B. Waltzman, “The effects of residual hearing in traditional cochlear implant candidates after implantation with a conventional electrode,” Otol. Neurotol. Off. Publ. Am. Otol. Soc. Am. Neurotol. Soc. Eur. Acad. Otol. Neurotol., vol. 34, no. 3, pp. 516–521, Apr. 2013.

[60] T. Lenarz, T. Stöver, A. Buechner, A. Lesinski-Schiedat, J. Patrick, and J. Pesch, “Hearing conservation surgery using the Hybrid-L electrode. Results from the first clinical trial at the Medical University of Hannover,” Audiol. Neurootol., vol. 14 Suppl 1, pp. 22–31, 2009.